Applied Physics Letters

Temperature-dependent phonon mode and interband electronic transition evolutions of ε-InSe films derived by pulsed laser deposition

Cite as: Appl. Phys. Lett. **117**, 102101 (2020); https://doi.org/10.1063/5.0021330
Submitted: 09 July 2020 . Accepted: 28 August 2020 . Published Online: 08 September 2020

Mingzhang Xie (谢明章), Ming Li (李明), Liumeng Li (李留猛), Jinzhong Zhang (张金中), Kai Jiang (姜凯), Liyan Shang (商丽燕), Yawei Li (李亚巍), Zhigao Hu (胡志高), and Junhao Chu (褚君浩)

Applied Physics Letters ARTICLE scitation.org/journal/apl

Temperature-dependent phonon mode and interband electronic transition evolutions of ε-InSe films derived by pulsed laser deposition

Cite as: Appl. Phys. Lett. **117**, 102101 (2020); doi: 10.1063/5.0021330
Submitted: 9 July 2020 · Accepted: 28 August 2020 ·
Published Online: 8 September 2020

Mingzhang Xie (谢明章),[1] Ming Li (李明),[1] Liumeng Li (李留猛),[1] Jinzhong Zhang (张金中),[1] Kai Jiang (姜凯),[1] Liyan Shang (商丽燕),[1] Yawei Li (李亚巍),[1] Zhigao Hu (胡志高),[1,2,3,a)] and Junhao Chu (褚君浩)[1,2,3]

AFFILIATIONS

[1]Technical Center for Multifunctional Magneto-Optical Spectroscopy (Shanghai), Engineering Research Center of Nanophotonics and Advanced Instrument (Ministry of Education), Department of Materials, School of Physics and Electronic Science, East China Normal University, Shanghai 200241, China

[2]Collaborative Innovation Center of Extreme Optics, Shanxi University, Taiyuan, Shanxi 030006, China

[3]Shanghai Institute of Intelligent Electronics and Systems, Fudan University, Shanghai 200433, China

[a)]Author to whom correspondence should be addressed: zghu@ee.ecnu.edu.cn

ABSTRACT

We report the temperature-dependent phonon modes and interband electronic transitions of InSe films on SiO_2/Si substrates prepared by pulsed laser deposition. The microstructure results proved the ε phase structure and monochalcogenide phase composition with well-defined hexagonal InSe sheets. The temperature effects on lattice vibrations were discovered by Raman spectra from 123 K to 423 K. The frequency and full width at half maximum of the A_{2g}^1(LO) mode show a strong nonlinearity with the temperature. The energy band structure and electron–phonon interaction were studied by temperature-dependent spectroscopic ellipsometry with the aid of the Tauc–Lorentz model. It was found that five electronic transitions around 1.33, 1.61, 2.53, 3.73, and 4.64 eV generally show a redshift trend with the temperature. The present results can provide a valuable reference for future optoelectronic applications of InSe films.

Since graphene has been found, two-dimensional (2D) materials as promising materials for next-generation semiconductor devices have been extensively studied, such as transition metal dichalcogenides, III–VI binary chalcogenides, black phosphorus, and so on.[1–4] Among them, InSe attracts a lot of attention due to its unique optical and electrical properties. The bandgap of InSe can be tunable between 1.2 and 2.2 eV with the thickness due to the quantum confinement, making it a potential material for optoelectronic applications from the infrared to visible light range.[5–10] The low electron effective mass and weak electron–phonon scattering give it an electron mobility up to 1000 $cm^2\ V^{-1}\ s^{-1}$, which can be extensively applied in field effect transistors (FETs).[3,4,11,12]

Traditionally, the way to obtain 2D material nanosheets is to peel them from the bulk or synthesize them by chemical vapor deposition (CVD), which cannot make large area films and stable output.[13] Recently, the pulsed laser deposition (PLD) method has provided a way for making large-area films.[7,14] Yang *et al.* have employed PLD to grow InSe films on SiO_2/Si substrates and studied the structure and optical and electrical properties. 1 nm InSe-based FETs have a mobility of 10 $cm^2\ V^{-1}\ s^{-1}$, which can be comparable to those synthesized by CVD.[7,12] Moreover, we have also grown high-quality MoS_2 and InSe films on mica using the PLD method. Through the annealing process, the molybdenum oxide and sulfur vacancies had been significantly reduced. The results from Raman, photoluminescence (PL), and x-ray diffraction (XRD) spectra proved the improved crystallinity after the annealing process. By using copper as the electrodes, the copper diffusion in InSe forms a $CuInSe_2$/InSe isotype heterojunction, which can improve the contact performance and photoelectric response.[15,16]

Although the temperature effect on lattice vibrations of 2D materials has been widely studied, the phonon frequency variations with the temperature have not been well clarified, especially for the InSe system. It is also found that the substrates have an influence on the temperature coefficient of the phonon frequencies.[17–21] The temperature-dependent Raman spectrum is a common method to study the variations of phonons with the temperature. On the other hand, InSe has a complicated nature of the energy band structure,

which makes it difficult to identify the origins of the electron transitions.[22–25] Therefore, it is necessary to study the vibrational properties and band structure of InSe films prepared by the PLD method, which may further estimate the photoelectric characteristics and transport properties.

In this Letter, we prepared InSe films on SiO_2/Si substrates using the PLD method. A pulsed KrF excimer laser (248 nm) with an energy fluence of 5 J cm^{-2} with a repetition rate of 10 Hz was used to ablate the commercial target with an In/Se ratio of 1:1. The chamber was kept at a vacuum of 5×10^{-6} mbar. The substrate was heated to 350 °C, and the holder was rotated during deposition. After deposition, the films are cooled down naturally to room temperature (RT). XRD (D/MAX-2550 V, Rigaku Co), x-ray photoelectron spectroscopy (XPS, RBD upgraded PHI-5000C ESCA system, PerkinElmer), Raman spectroscopy (Jobin-Yvon LabRAM HR Evolution), and Spectroscopic ellipsometry (SE) measurements were carried out to investigate the crystalline, compositions, valence, and band structure of InSe films.

Figure 1(a) shows the diffraction pattern of the film deposited on SiO_2/Si. Compared to the diffraction pattern of the substrate, there are four diffraction peaks from the film. All peaks agree with the (002), (004), (006), and (008) orientations (JCPDS No. 34–1431) of InSe, indicating the β or ε phase. From Fig. 1(b), it is found that the peaks

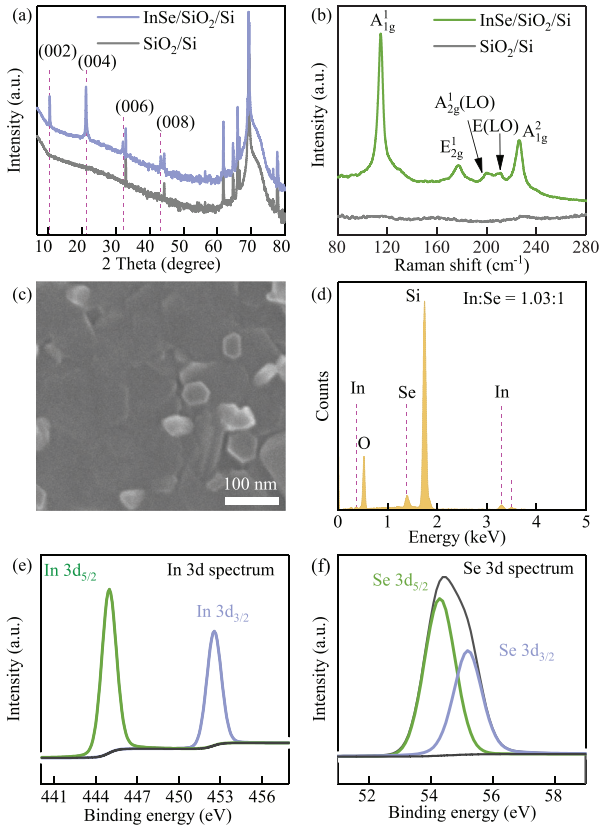

FIG. 1. (a) XRD patterns and (b) Raman spectra of the InSe film and substrate, respectively. (c) The SEM image of the film surface with a hexagonal stacking structure. (d) EDS mapping on Se and In elements. The XPS experiment data and fitting results of (e) In $3d_{5/2}$ and (f) Se $3d_{3/2}$.

located around 114.8, 176.8, 200.5, 209.5, and 226.5 cm^{-1} correspond to the A^1_{1g}, E^1_{2g}, A^1_{1g}(LO), E(LO), and A^2_{1g} modes, respectively.[26] The A^1_{1g}, E^1_{2g}, and A^2_{1g} modes originate from the zone center vibrational modes, and the A^1_{1g}(LO) and E(LO) modes result from the resonance effect. The A^1_{1g}(LO) and E(LO) modes are only related to the γ and ε phase.[8] Therefore, combining the results from XRD patterns and Raman spectra, we think that the InSe film in the present work is of the ε phase. The SEM image in Fig. 1(c) demonstrates the hexagonal stacking structure on the film surface. Energy dispersive (EDS) mapping in Fig. 1(d) shows the chemical composition of In and Se, confirming the monochalcogenide phase of the InSe film.[7] Figures 1(e) and 1(f) show the XPS spectra of the In 3d level and Se 3d level. The doublet peaks around 444.9 and 452.5 eV are attributed to the In $3d_{5/2}$ and In $3d_{3/2}$ states of InSe with a peak separation of 7.6 eV. The doublet peaks around 54.3 eV and 55.2 eV belong to Se $3d_{5/2}$ and Se $3d_{3/2}$ with a spin–orbit split of 0.9 eV.[12] No peaks from the Se–O bonds were found in the XPS results.

Figure 2(a) shows the optical image of the InSe film. Raman mapping for the peak intensity of the A^1_{1g} mode from a 40 μm × 40 μm area was performed to evaluate the uniformity of the film. As shown in Fig. 2(b), the surface of the substrate is fully covered with the InSe film and the intensity is distributed between 1000 and 1500 under the same laser excitation. Temperature-dependent Raman spectra from 123 K to 423 K were obtained in this area, as shown in Fig. 2(c). By means of fitting the experimental data using the Lorentzian functions, the peak position and full width at half maximum (FWHM) were obtained from each spectrum. From Fig. 2(d), it is found that the vibration frequency of Raman modes decreases monotonously with the increasing temperature. The peak positions were fitted using the formula:[27] $\omega(T) = \omega_0 + \chi_1 T + \chi_2 T^2 + \chi_3 T^3$, where ω_0 is the peak position of A^1_{1g}, E^1_{2g}, A^1_{2g}(LO), E(LO), and A^2_{1g} modes at 0 K and χ_1, χ_2, and χ_3 are the first, second, and third order temperature coefficient of each mode. The χ_1 values for each mode are −0.004, −0.009, −0.06, −0.004, and −0.012 cm^{-1} K^{-1}, respectively. The more linear the peak position changes with the temperature, like A^1_{1g} and A^2_{1g} modes, the lower the higher-order temperature coefficient is. The second-order temperature coefficients of the A^1_{2g}(LO) and E(LO) modes are an order of magnitude higher than those of the A^1_{1g} and A^2_{1g} modes. The changes in frequencies can be mostly attributed to the thermal expansion of the lattice and anharmonicity effects. The strong nonlinearity of the A^1_{2g}(LO) and E(LO) modes may be related to their origin, which causes stronger anharmonic vibration than the others. Figure 2(e) shows the temperature-dependent FWHM of each mode. These values are little larger than those from single crystals, which may indicate the existence of defects.[26] In general, the FWHM of A^1_{1g}, E^1_{2g}, E(LO), and A^2_{1g} modes increases with the temperature. However, the A^1_{2g}(LO) mode does not act linearly and reaches its maximum value near room temperature (RT). The mismatch of thermal expansion coefficients between the InSe film and the SiO_2/Si substrate gives rise to changes of morphology, which may lead to a significant change in the temperature coefficient χ for the A^1_{2g}(LO) mode.[27] As the temperature increases, it is found that the intensity of some peaks changes regularly. Therefore, in order to explore the law of peak intensity evolutions, we normalize the Raman spectra to have the same peak intensity for the A^1_{1g} mode and define the ratio of E^1_{2g}, A^1_{2g}(LO), E(LO), A^2_{1g}, and A^1_{1g} mode intensity as the relative intensity. The relative intensity of the E^1_{2g}, A^1_{2g}(LO), and E(LO) modes increases with the temperature,

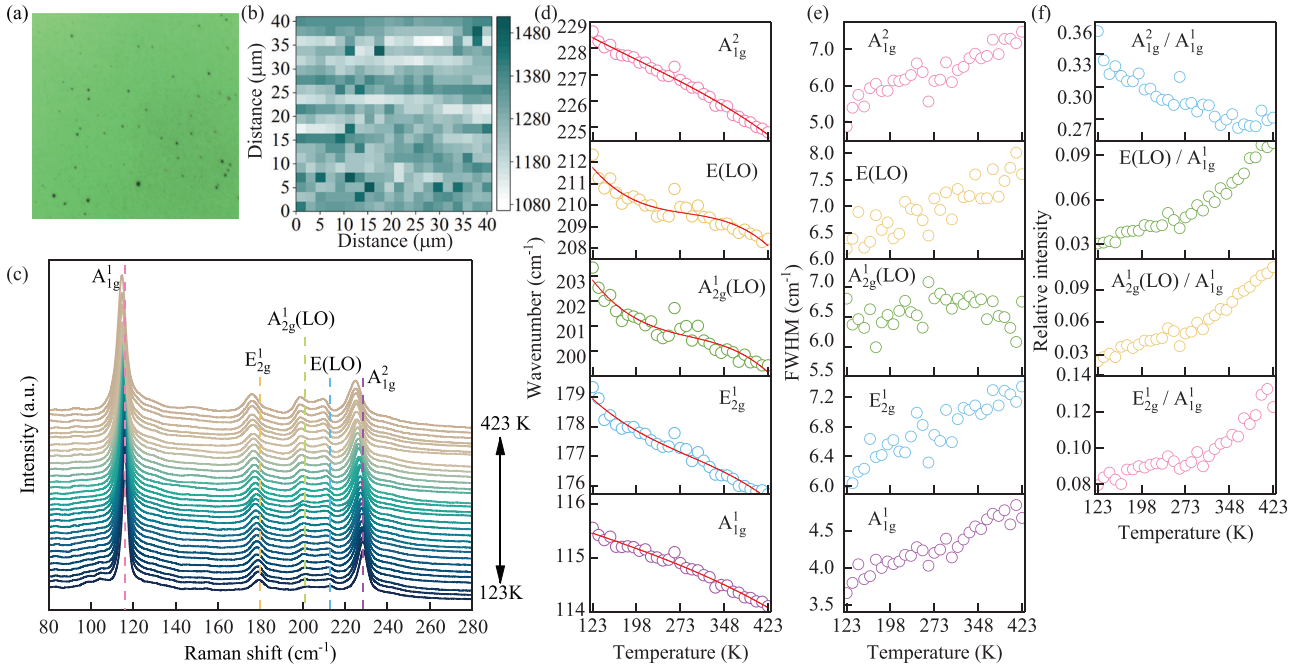

FIG. 2. (a) Optical image of the InSe film. (b) Raman mapping for the peak intensity of A^1_{1g} mode from a 40 μm × 40 μm area. (c) Temperature-dependent Raman spectra from 123 K to 423 K. (d) The evolution of A^1_{1g}, E^1_{2g}, A^1_{2g}(LO), E(LO), and A^2_{1g} modes with the temperature. (e) The FWHM variation of A^1_{1g}, E^1_{2g}, A^1_{2g}(LO), E(LO), and A^2_{1g} modes with the temperature. (f) The relative intensity of E^1_{2g}, A^1_{2g}(LO), E(LO), and A^2_{1g} modes to A^1_{1g} mode with the temperature.

except for the A^2_{1g} mode. Song *et al.* found that uniaxial tensile strain will cause peaks to redshift and dramatically enhance the A^1_{2g}(LO) and E(LO) modes of γ-InSe, which has a similar phenomenon to that in the present work.[28] We think that the strain induced by the lattice expansion with the temperature should be mostly responsible for the enhancement of the E^1_{2g}, A^1_{2g}(LO), and E(LO) modes.

Spectroscopic ellipsometry is a noninvasive and sensitive optical method to characterize the dielectric functions of condensed matter materials. The distinct electronic transition patterns together with charge transfers can be extracted from the spectra.[29,30] Figure 3(a) shows the experimented pseudodielectric function: $\langle\tilde{\varepsilon}(E)\rangle = \langle\varepsilon_1(E)\rangle + i\langle\varepsilon_2(E)\rangle$ of InSe/SiO_2/Si at 123 K, 223 K, 273 K, 323 K, and 423 K, respectively. Upon increasing the temperature, the peaks have a redshift. In this work, a four-layer model (roughness/InSe/SiO_2/Si) was used to simulate the complex dielectric function of the InSe film. Five Tauc–Lorentz (TL) oscillators were applied to express the optical response of the InSe film. The expression of the TL model is given by[30] $\varepsilon_1(E) = \varepsilon_\infty + \frac{2}{\pi} P \int_{E_t}^{\infty} \frac{\xi\varepsilon_2(\xi)}{\xi^2 - E^2} d\xi$; $\varepsilon_2(E) = \frac{AE_nC(E-E_t)^2}{(E^2-E_n^2)^2+C^2E^2}\frac{1}{E}$ $(E \geq E_t)$ and $\varepsilon_2(E) = 0$, $(E < E_t)$, where the P is the Cauchy principal part of the integral, ε_∞ is the high frequency dielectric constant, and E is the incident photon energy. The parameters A, E_n, C, and E_t are the amplitude, peak position energy, broadening term, and Tauc gap energy, respectively. The TL parameter values of the InSe film at RT are listed in Table I. The five optical transition peaks named $TL_{j\,=\,1\text{–}5}$ at RT are located at 1.33, 1.61, 2.53, 3.73, and 4.64 eV, respectively. According to the results of theoretical calculations and optical studies on single crystals, the five oscillators can be explained as follows. The TL_1 (1.33 eV) corresponds to the transition from the top of the valence band (Se p_z) to the bottom of the conduction band at the Γ point of the Brillouin zone (BZ), close to the values from the theoretical calculation and optical test.[10,24] Mostly due to the quantum confinement effect, the bandgap here is larger than that of the bulk. As the conduction band minimum of In_2O_3 lies above that of InSe by 0.29 eV,[31,32] the TL_2 (1.61 eV) may be related to the impurity level introduced by indium oxide in the conduction band. The TL_3 (2.53 eV) in the table is from the excitation of Se P_xP_y electrons to the conduction band minimum. The energy separation between the highest valence band Se p_z and the second highest valence band Se P_xP_y is 1.2 eV, which agrees with the results obtained from the single crystal. The TL_4 (3.73 eV) may come from the valence band maximum to the third group of the conduction band at or near the Γ point. The TL_5 (4.64 eV) may be related to the excitation from the second highest valence band to either the second or the third group of conduction bands.[22,33] These assignments from SE data could be helpful for clarifying the physical origin.

Figure 3(b) shows the second derivatives of pseudodielectric function $\langle\varepsilon_1\rangle$ and $\langle\varepsilon_2\rangle$ at RT from the experimental data (dotted) and the best fitting curves (solid lines). The ε_1 and ε_2 values of InSe were obtained from the fitting results, as shown in Fig. 3(c) from 0.9 eV to 5 eV. The highest peak of ε_2 around 2.5 eV corresponds to the strongest absorption, related to electronic transition from the Se P_xP_y level to the minimum conduction band. As shown in Fig. 3(d), the energy of oscillators generally has a redshift with the temperature, consistent with the previous observations. It is well known that the electron–phonon interaction and the lattice thermal expansion are related to

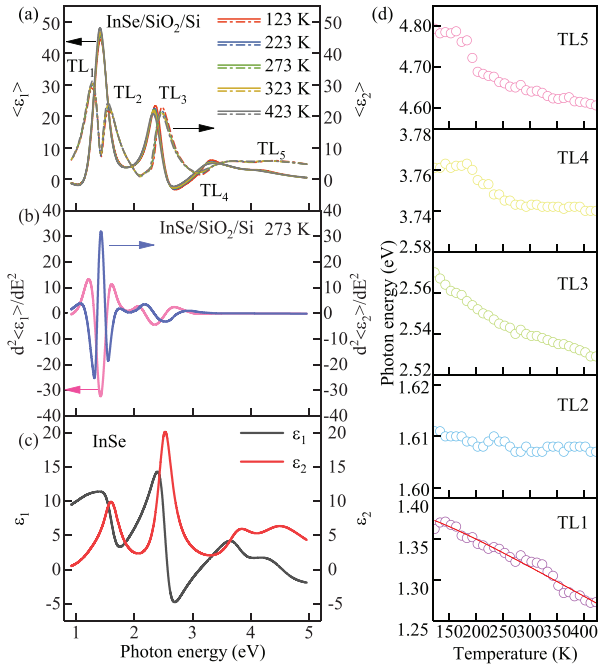

FIG. 3. (a) The experimented real parts $\langle\varepsilon_1\rangle$ and imaginary parts $\langle\varepsilon_2\rangle$ of pseudodielectric functions measured at 123 K, 223 K, 273 K, 323 K, and 423 K, respectively. (b) The experimental (dotted) and the best fitting (solid lines) second derivatives of pseudodielectric function $\langle\varepsilon_1\rangle$ and $\langle\varepsilon_2\rangle$ at RT. (c) The real (ε_1) and imaginary (ε_2) parts of dielectric functions of InSe extracted from the fitting results. (d) The energy variations of five Tauc–Lorentz oscillators with the temperature. Note that the TL1 transition can be fitted using the Bose–Einstein model (solid line).

the energy redshift of electronic transitions. The TL_1 and TL_5 transitions have the larger variations than the others, which indicate the difference in the effects of electron–phonon interaction and thermal expansion on different electronic transitions. A Bose–Einstein model was used to describe the electron–phonon coupling of the TL_1 oscillator, given as $E_{OBG}(T) = E_{OBG}(0) - a_B/[\exp(\Theta_B/T) - 1]$,[29] where $E_{OBG}(0)$ is the optical bandgap at $T = 0$ K, a_B represents the strength of the electron–phonon interaction, and Θ_B corresponds to the average phonon temperature, i.e., the Einstein characteristic temperature. The parameters $E_{OBG}(0)$, a_B, and Θ_B are estimated to be 1.385 eV, 0.101 eV, and 270 K, respectively. The estimated parameters for single crystals are 1.336 eV, 0.059 eV, and 262 K.[34] Compared to the results estimated from single crystals, the film here has a larger calculated bandgap at 0 K, which can be mostly attributed to the thinner film thickness. Also, the larger a_B means larger strength of electron–phonon interaction, which can be attributed to the more defects of the films than that from single crystals. For the TL_2, TL_3, and TL_4 oscillators, the smaller energy changes with the temperature may be due to smaller strength of the electron–phonon interaction. Based on the above Raman spectra, there are five phonons around 114.8, 176.8, 200.5, 209.5, and 226.5 cm^{-1}, respectively. Compared to single crystals, the average phonon frequency of the film also includes the influence from the substrate. The average phonon value here is about 188–184 cm^{-1} from 123 K to 423 K, corresponding to an Einstein characteristic temperature from about 271 K to 265 K, which agrees with the fitting result. The lattice thermal expansion is generally shifting the electronic structure linearly. As the temperature increases, the lattice expansion will increase the distance between atoms, weakening the interaction between atoms, which usually moves the conduction band downward and the valence band to move down.[29] This is consistent with the observation in our experiment. Li *et al.* found that the tensile strain would cause the Raman and photoluminescence peaks to redshift.[20] From the perspective of strain, the tensile strain introduced by heating, as well as the strain induced by the thermal expansion difference for the InSe film and substrates, may be the main cause of the optical bandgap variation, which echoes the analysis of the peak intensity change of the Raman modes.

In summary, we have studied the temperature effects on the phonon modes for ε-InSe films grown using the PLD method. The electronic transitions have been discovered by SE with the aid of the Tauc–Lorentz model. Using the Bose–Einstein model, we explained the variation of the optical bandgap with the temperature for the InSe film. The present study can promote further understanding of the phonons and electronic transitions for InSe films.

TABLE I. The Tauc–Lorentz parameter values of the InSe film at room temperature determined from SE. Note that the 90% reliability of the fitting parameters is given in parentheses.

Oscillator (TL_j)	A_j (eV)	E_nj (eV)	C_j (eV)	E_tj (eV)
$j = 1$	10.2	1.33	0.808	0.737
	(2.6)	(0.14)	(0.52)	(0.16)
$j = 2$	13.2	1.61	0.294	1.02
	(0.4)	(0.01)	(0.07)	(0.08)
$j = 3$	36.4	2.53	0.253	1.58
	(6.3)	(0.13)	(0.01)	(0.34)
$j = 4$	157	3.73	0.405	3.27
	(29)	(0.16)	(0.22)	(0.33)
$j = 5$	69.0	4.64	1.04	3.22
	(1.8)	(0.28)	(0.19)	(0.52)

This work was financially supported by the National Key R&D Program of China (Grant Nos. 2018YFB0406500, 2017YFA0303403, and 2019YFB2203400), the Natural Science Foundation of China (Grant Nos. 91833303, 61974043, 61805081, and 61674057), Projects of Science and Technology Commission of Shanghai Municipality (Grant Nos. 18JC1412400, 18YF1407200, 18YF1407000, and 19511120100), and the Program for Professor of Special Appointment (Eastern Scholar) at Shanghai Institutions of Higher Learning.

DATA AVAILABILITY

The data that support the findings of this study are available from the corresponding author upon reasonable request.

REFERENCES

[1]K. S. Novoselov, A. K. Geim, S. V. Morozov, D. Jiang, M. I. Katsnelson, I. V. Grigorieva, S. V. Dubonos, and A. A. Firsov, Nature **438**, 197 (2005).
[2]B. Radisavljevic, A. Radenovic, J. Brivio, V. Giacometti, and A. Kis, Nat. Nanotechnol. **6**, 147 (2011).

[3]D. A. Bandurin, A. V. Tyurnina, G. L. Yu, A. Mishchenko, V. Zólyomi, S. V. Morozov, R. K. Kumar, R. V. Gorbachev, Z. R. Kudrynskyi, S. Pezzini, Z. D. Kovalyuk, U. Zeitler, K. S. Novoselov, A. Patanè, L. Eaves, I. V. Grigorieva, V. I. Fal'ko, A. K. Geim, and Y. Cao, Nat. Nanotechnol. **12**, 223 (2017).
[4]S. W. Zhao, J. C. Wu, K. Jin, H. Y. Ding, T. S. Li, C. Z. Wu, N. Pan, and X. P. Wang, Adv. Funct. Mater. **28**, 1802011 (2018).
[5]G. W. Mudd, A. Patanè, Z. R. Kudrynskyi, M. W. Fay, O. Makarovsky, L. Eaves, Z. D. Kovalyuk, V. Zólyomi, and V. Falko, Appl. Phys. Lett. **105**, 221909 (2014).
[6]W. j Huang, L. Gan, H. Q. Li, Y. Ma, and T. Y. Zhai, Chem. Eur. J. **24**, 15678 (2018).
[7]Z. B. Yang, W. J. Jie, C. Mak, S. H. Lin, H. H. Lin, X. F. Yang, F. Yan, S. P. Lau, and J. H. Hao, ACS Nano **11**, 4225 (2017).
[8]S. D. Lei, L. H. Ge, S. Najmaei, A. George, R. Kappera, J. Lou, M. Chhowalla, H. Yamaguchi, G. Gupta, R. Vajtai, A. D. Mohite, and P. M. Ajayan, ACS Nano **8**, 1263 (2014).
[9]S. R. Tamalampudi, R. Sankar, H. Apostoleris, M. A. Almahri, B. Alfakes, A. Al-Hagri, R. Li, A. Gougam, I. Almansouri, M. Chiesa, and J. Y. Lu, J. Phys. Chem. C **123**, 15345 (2019).
[10]G. W. Mudd, S. A. Svatek, T. H. Ren, A. Patanè, O. Makarovsky, L. Eaves, P. H. Beton, Z. D. Kovalyuk, G. V. Lashkarev, Z. R. Kudryskyi, and A. I. Dmitriev, Adv. Mater. **25**, 5714 (2013).
[11]S. Sucharitakul, N. J. Goble, U. R. Kumar, R. Sankar, Z. A. Bogorad, F. C. Chou, Y. T. Chen, and X. P. A. Gao, Nano Lett. **15**, 3815 (2015).
[12]H. C. Chang, C. L. Tu, K. I. Lin, J. Pu, T. Takenobu, C. N. Hsiao, and C. H. Chen, Small **14**, 1802351 (2018).
[13]Z. Yang and J. Hao, J. Mater. Chem. C **4**, 8859 (2016).
[14]M. I. Serna, S. H. Yoo, S. Moreno, Y. Xi, J. P. Oviedo, H. Choi, H. N. Alshareef, M. J. Kim, M. Minary-Jolandan, and M. A. Quevedo-Lopez, ACS Nano **10**, 6054 (2016).
[15]H. Ji, M. Z. Xie, J. y Zhou, X. Wang, Z. Jin, K. Jiang, L. Y. Shang, Z. G. Hu, and J. H. Chu, Appl. Phys. Lett. **115**, 162104 (2019).
[16]M. Z. Xie, J. Y. Zhou, H. Ji, Y. Ye, X. Wang, K. Jiang, L. Y. Shang, Z. G. Hu, and J. H. Chu, Appl. Phys. Lett. **115**, 121901 (2019).
[17]I. Calizo, A. A. Balandin, W. Bao, F. Miao, and C. N. Lau, Nano Lett. **7**, 2645 (2007).
[18]D. J. Late, ACS. Appl. Mater. Interfaces **7**, 5857 (2015).
[19]A. S. Pawbake, M. S. Pawar, S. R. Jadkar, and D. J. Late, Nanoscale **8**, 3008 (2016).
[20]Y. Li, T. M. Wang, M. Wu, T. Cao, Y. W. Chen, R. Sankar, R. K. Ulaganathan, F. C. Chou, C. Wetzel, C. Y. Xu, S. G. Louie, and S. F. Shi, 2D Mater. **5**, 021002 (2018).
[21]V. D. Botcha, M. Zhang, K. L. Li, H. Gu, Z. H. Huang, J. H. Cai, Y. M. Lu, W. J. Yu, and X. K. Liu, J. Alloys Compd. **735**, 594 (2018).
[22]J. V. McCanny and R. B. Murray, J. Phys. C **10**, 1211 (1977).
[23]S. J. Magorrian, V. Zólyomi, and V. I. Fal'ko, Phys. Rev. B **94**, 245431 (2016).
[24]M. O. D. Camara, A. Mauger, and I. Devos, Phys. Rev. B **65**, 125206 (2002).
[25]D. K. Sang, H. D. Wang, M. Qiu, R. Cao, Z. N. Guo, J. L. Zhao, Y. Li, Q. L. Xiao, D. Y. Fan, and H. Zhang, Nanomaterials **9**, 82 (2019).
[26]F. F. Chen, A. Y. Cui, X. Wang, C. F. Gao, L. P. Xu, K. Jiang, J. Z. Zhang, Z. G. Hu, and J. H. Chu, Nanotechnology **31**, 335702 (2020).
[27]L. Q. Su, Y. Zhang, Y. F. Yu, and L. Y. Cao, Nanoscale **6**, 4920 (2014).
[28]C. Y. Song, F. R. Fan, N. N. Xuan, S. Y. Huang, C. Wang, G. W. Zhang, F. J. Wang, Q. X. Xing, Y. C. Lei, Z. Z. Sun, H. Wu, and H. G. Yan, Phys. Rev. B **99**, 195414 (2019).
[29]M. J. Han, K. Jiang, J. Z. Zhang, Y. W. Li, Z. G. Hu, and J. H. Chu, Appl. Phys. Lett. **99**, 131104 (2011).
[30]S. Guo, X. J. Ding, J. Z. Zhang, Z. G. Hu, X. L. Ji, L. C. Wu, Z. T. Song, and J. H. Chu, Appl. Phys. Lett. **106**, 052105 (2015).
[31]O. Lang, C. Pettenkofer, J. F. Sánchez-Royo, A. Segura, A. Klein, and W. Jaegermann, J. Appl. Phys. **86**, 5687 (1999).
[32]N. Balakrishnan, Z. R. Kudrynskyi, E. F. Smith, M. W. Fay, O. Makarovsky, Z. D. Kovalyuk, L. Eaves, P. H. Beton, and A. Patanè, 2D Mater. **4**, 025043 (2017).
[33]S. G. Choi, D. E. Aspnes, A. L. Fuchser, C. Martinez-Tomas, V. M. Sanjosè, and D. H. Levi, Appl. Phys. Lett. **96**, 181902 (2010).
[34]B. Abay, H. S. Güder, H. Efeoğlu, and Y. K. Yoğurtcu, J. Phys. D **32**, 2942 (1999).